Massively Multipoint Aerodynamic Shape Design via Surrogate-Assisted Gradient-Based Optimization

Jichao Li* and Jinsheng Cai†
Northwestern Polytechnical University, 710072 Xi'an, People's Republic of China

https://doi.org/10.2514/1.J058491

Multipoint aerodynamic design optimization involves no more than tens of flight conditions, which cannot thoroughly represent the actual demand. A comprehensive evaluation of the performance may consider hundreds or even thousands of flight conditions, and this leads to a massively multipoint optimization problem. Existing optimization methods are inefficient in such cases. This paper presents a surrogate-assisted gradient-based optimization architecture that efficiently solves massively multipoint design problems. To avoid the curse of dimensionality, surrogate models are constructed only in the low-dimensional space spanned by flow condition variables. With the aerodynamic functions and gradients computed by surrogate models, efficient gradient-based optimization is performed to find the optimal design. To ensure convergence, an adaptive sampling criterion is proposed to refine the surrogate models. In a transonic aircraft wing design case, the results show that the optimal design found by the proposed method with 342 missions yields a fuel burn reduction by a factor of two as compared to a regular multipoint optimal design. This work highlights the demand and provides an efficient way to conduct massively multipoint optimization in aircraft design.

Nomenclature

C_d	=	drag coefficient
C_l	=	lift coefficient
f	=	objective function
f_a	=	aerodynamic constraint
f_δ	=	regressed error
$g(\boldsymbol{x}_s)$	=	geometric constraints
$\tilde{L}$	=	likelihood function
M	=	Mach number
R	=	covariance matrix of kriging
R	=	flight mission range
R_{Fuel}	=	fuel burn reduction ratio
$R(\boldsymbol{x}, \boldsymbol{x}')$	=	kernel function of kriging
S	=	wing area
s^2	=	mean squared error
t	=	thickness
t/c	=	relative thickness
V	=	wing volume
W	=	weight
w^i	=	combination coefficient of the ith design point
$\boldsymbol{x}$	=	input variables
$\boldsymbol{x}_f$	=	flow condition variables
$\boldsymbol{x}_s$	=	shape design variables
α	=	angle of attack
$\delta^{(k)}$	=	variation of the prediction in the kth infill sampling step
ε	=	projection error
κ	=	error threshold for the infill sampling process termination
Λ	=	wing sweep angle

Received 20 March 2019; revision received 1 November 2019; accepted for publication 6 November 2019; published online 30 December 2019.

*cfdljc@gmail.com. Member AIAA.

†Professor, National Key Laboratory of Aerodynamic Design and Research, Department of Fluid Mechanics, School of Aeronautics, Shaanxi; caijsh@nwpu.edu.cn. Senior Member AIAA.

I. Introduction

AERODYNAMIC shape optimization with numerical simulations has led to higher efficiency and shorter development cycles in aircraft design, and different optimization methods [1–3] have been developed to satisfy requirements in different design stages. Due to the high computational cost of computational fluid dynamics (CFD) analyses, gradient-based optimization algorithms are preferable when the aerodynamic coefficients are directly evaluated by CFD. This kind of method is efficient when the adjoint method [4–10] is used to solve the gradient. Zingg and Elias [11] conducted gradient-based design optimization of airfoils under a range of conditions. Lyu et al. studied the aerodynamic optimization of the NASA Common Research Model (CRM) wing [12] and a blended-wing/body aircraft [13] with an adjoint solver of the Reynolds-averaged Navier–Stokes equations [7]. Recently, the development of open-source computational fluid dynamics codes with adjoint solvers, like SU2 [14] and ADflow [15], makes it more accessible to conduct gradient-based aerodynamic optimization. Alternatively, one can adopt the complex-step method [16] to accomplish the gradient-based optimization in cases without adjoint solvers. In addition, surrogate-based optimization [3,17–20] is also a popular approach in aircraft design, where aerodynamic functions are evaluated with computationally cheap surrogate models in place of CFD models [21]. The drawback of surrogate-based optimization is the curse of dimensionality, and its application in high-dimensional cases was restricted [22,23]. To address this issue, Li et al. [3] applied the active subspace method in surrogate-based optimization and made it efficient and applicable in the wing design optimization with hundreds of shape design variables.

Nevertheless, new optimization methodologies are still in demand to provide more robust designs with highly improved quality [24]. Aerodynamic design optimization is driven by tradeoffs [25], and single-point optimization could overstate the benefits of the optimization by reducing the performance at offdesign points [12]. Li et al. [26] proposed a data-driven constraint to account for the influence of offdesign points, and this constraint makes the transonic design optimization robust in the subsonic regime as well. More generally, multipoint optimization [2,11,27–32] is adopted to involve tradeoffs and improve design robustness. The computational cost of multipoint optimization increases linearly with the number of design points. So, several ($5 \sim 25$) design points are generally used in regular multipoint optimization. However, the optimal design that fits the actual demand should consider missions more comprehensively [33]. Figure 1 shows 529 mission frequencies of the Boeing 777-200ER based on

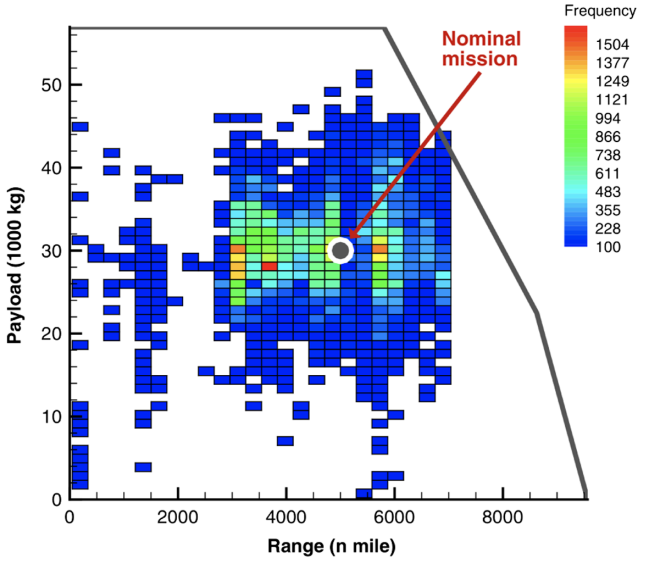

Fig. 1 The 529 flight missions [34] lead to a massively multipoint optimization problem.

real flight data, which Liem et al. [34] extracted from the Bureau of Transportation Statistics' flight database. Although 25 flight conditions were used in the optimization [34], these missions yield an optimization problem with a large number of (529) design points that we refer to as a massively multipoint optimization problem. Chai et al. [35] performed a 426-point optimization of a wide-body aircraft using a low-fidelity aerodynamic model and quasi-analytical techniques. The optimal design achieved a higher fuel efficiency than the single-point optimum.

However, in the context of massively multipoint design optimization with high-fidelity aerodynamic models, both gradient-based optimization and surrogate-based optimization are inefficient. The objective function in a massively multipoint optimization problem is a mixture of aerodynamic functions under a large set of flight conditions. So, the evaluation of it needs massive CFD simulations, which lead to a huge computational cost. Gradient-based optimization in this situation becomes costly, even with an efficient adjoint solver. Surrogate-based optimization could be advantageous in such cases because the objective and constraint functions can be fast evaluated by surrogate models. However, the number of design variables can be hundreds or even thousands in wing and aircraft design optimization. Surrogate models cannot scale well in such high-dimensional problems. The active subspace assisted surrogate-based optimization method proposed by Li et al. [3] addresses the curse of dimensionality in the early design stage, but its performance in the detail design phase has not been investigated yet. Liem et al. [36] investigated constructing surrogate models of aerodynamic functions using the mixture of experts in the design space of several flow variables; but, for massive shape design variables, the performance of this strategy has not been studied. Other studies sought to address this issue by simplifying massively multipoint optimization problems. Liem et al. [34] modified the objective function to a weighted combination of several design points that were automatically selected based on the flight data. Thus, the difficult massively multipoint optimization was transferred to a multipoint optimization problem. Liem et al. [37] also investigated the selection of flight conditions and their weights based on a flight-condition probability density function. Jacome and Elham [38] transferred the massively multipoint design problem to an optimization problem with uncertainty. This allowed avoidance of the evaluations of all design points. These approaches have been verified in the aerostructural optimization of aircraft wings [34,37,38]. Nevertheless, the influence of these simplifications has not yet been investigated. The potential impact could be unpredictable because aircraft design involves complex and strongly nonlinear phenomena [32]. Thus, an optimization architecture that strictly and efficiently solves the massively multipoint design problem is still in demand.

We propose an approach that efficiently performs the gradient-based optimization with the assistance of surrogate models in massively multipoint design problems. We notice that the diversity among different design points is due to flow condition variables (for example, the angles of attack and Mach numbers), and their number of dimensions is low. Shape design variables result in high dimensionality, but they do not change in different design points. To reduce the computational cost, we alternatively construct surrogate models in the space spanned by flow condition variables. These surrogate models, including gradient-enhanced kriging (GEK) and kriging with the proper orthogonal decomposition (POD) (hereafter referred to as POD kriging), provide fast approximations of aerodynamic functions and their gradients. To efficiently refine these surrogate models, we present an adaptive sampling method based on the estimated error. Then, we conduct gradient-based optimization in the space of all design variables. Surrogate models are reconstructed in each gradient-based optimization iteration after the aerodynamic shape is updated. This optimization architecture takes advantage of surrogate models without suffering from the curse of dimensionality. It also benefits from the high efficiency of gradient-based optimization in the high-dimensional design space. We use this method in the design optimization of an aircraft wing, and the results demonstrate that the massively multipoint design optimization brings more benefits than commonly used multipoint optimization.

The rest of this paper is organized as follows: First, we describe the massively multipoint aerodynamic shape optimization problem to reduce the fuel burn in aircraft design (Sec. II). We propose the massively multipoint optimization method and discuss the details in Sec. III. Then, we adopt this method in the airfoil and wing shape design optimization to reduce the total fuel burn among different missions (Sec. IV). We end this paper with a summary of conclusions (Sec. V).

II. Optimization Problem Description

The design of next-generation aircraft should thoroughly consider actual flight conditions, which calls for massively multipoint design optimization. In this work, we perform a massively multipoint optimization in the aerodynamic shape design of a commercial aircraft wing to reduce the total fuel burn among different missions. The flight mission data are downloaded from the Bureau of Transportation Statistics (BTS) database, as Liem et al. [34] did. We extract payload and range data of the Boeing 787-800 aircraft in 116,327 missions during the past five years (from 2013 to 2017). These missions are summarized into 342 design points. The fuel burn is evaluated using the Breguet range equation [34,39,40]. We compute the combination coefficient w^i of each design point using the mission frequency shown in Fig. 2.

We describe the massively multipoint wing design optimization case in Sec. II.A. To validate algorithms with a lower computational cost, we also introduce an airfoil design optimization case in Sec. II.B, which is a simplification of the wing optimization case.

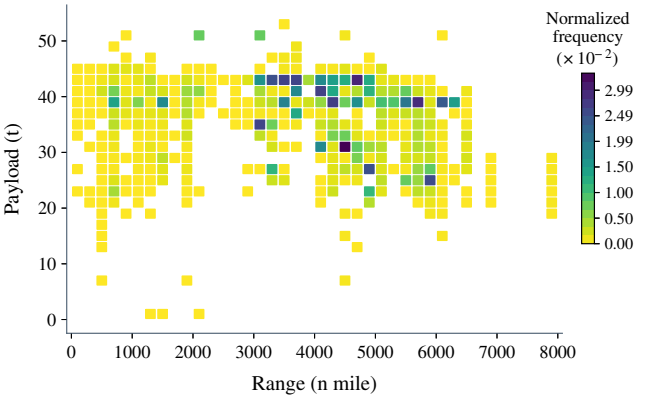

Fig. 2 Histogram of 116,327 flights for the Boeing 787-800 aircraft based on the BTS data.

A. Wing Shape Design Optimization

As shown in Fig. 3, we create a baseline wing by referring to the B787-800 aircraft. The wing dihedral is based on the CRM wing [41], and the wing section shape is scaled with the RAE 2822 airfoil. Other parameters of the baseline wing are specified in Table 1. As shown in Fig. 3b, we parameterize the baseline wing shape using the freeform deformation (FFD) method [42] with $2 \times 9 \times 9$ control points. We allow the change of wing sections, twist angles, and the sweep angle. However, the wingspan, taper, and area are fixed during the optimization to make a concise test case. We understand that this choice may not be appropriate in a practical aircraft design context. Nevertheless, it is sufficient to validate the proposed optimization architecture.

The cruise lift should be equal to the total weight, which is computed with the mission payload W^i_{Payload}:

$$C^i_{L,\text{cruise}} = \frac{L^i}{0.5\rho V^2 S} = \frac{(W^i_{\text{Payload}} + W_{\text{OEW}} + W_{\text{Fuel}}) \times g}{0.5 \times \rho_{\text{cruise}} \times (M_{\text{cruise}} \times a_{\text{cruise}})^2 \times S_{\text{ref}}} \quad (1)$$

where the speed of sound and air density at the cruise altitude are $a_{\text{cruise}} = 296.535$ m/s and $\rho_{\text{cruise}} = 0.379597$ kg/m^3 based on the U.S. Standard Atmosphere 1976 [43]. Gravitational acceleration is approximately $g = 9.8$ m/s^2. We use an estimation of the fuel weight with $W_{\text{Fuel}} = 10 \times R$ kg to compute lift constraints, where R is the mission range in units of a nautical miles. This assumption is obtained by regressing Eq. (2) with the typical cruise lift coefficient ($C_L = 0.5$) of the baseline aircraft. We use it to fast estimate the W_{Fuel} term in Eq. (1). This assumption does not consider the changes in the lift coefficient and payload, which may lead to inaccuracy. An accurate estimation of the fuel burn can be found in Ref. [44]. Figure 4 shows the $C^i_{L,\text{cruise}}$ of each mission, and we use them as lift constraints in the optimization. Besides, we only compute the aerodynamic force of the wing, and so we add 100 drag counts to the computed C_D in Eq. (2) to account for the aerodynamic influence of other components like the fuselage [12]. Then, the fuel burn in this wing design optimization case is estimated by

$$W_{\text{Fuel}} = (W_{\text{Payload}} + W_{\text{Wing}} + W_{\text{Rest}}) \left(\exp\left(R \frac{g \times \text{SFC}}{V} \frac{C_D + 0.01}{C_L} \right) - 1 \right) \quad (2)$$

The explanation of Eq. (2) is given in the Appendix.

Table 2 describes this massively multipoint optimization problem. Apart from this optimization, we also conduct a single-point optimization and regular multipoint optimization as comparisons. The mission condition of the single-point optimization ($\text{Payload}^{(\text{single})} = 36$ t, $\text{Range}^{(\text{single})} = 4100$ n miles) is the weighted average of 342 mission conditions, i.e.,

Table 1 Specifications of the baseline aircraft

Parameters	Value
Cruise Mach number M_{cruise}	0.85
Cruise altitude	35,000 ft
Reference wing area S_{ref}	325 m^2
Aspect ratio	9.0
$(t/c)_{\text{rep}}$	0.121
Quarter-chord sweep angle	32.2°
Maximum takeoff mass (MTOW)	228,000 kg
Operational empty weight W_{OEW}	118,000 kg
SFC	16×10^{-6} kg/(N · s)

$$\text{Payload}^{(\text{single})} = \sum_{i=1}^{342} w^i \times \text{Payload}^{(i)}$$
$$\text{Range}^{(\text{single})} = \sum_{i=1}^{342} w^i \times \text{Range}^{(i)} \quad (3)$$

The multipoint optimization involves five flight conditions: one is the ondesign point of the single-point optimization and the other four are perturbed around it ($\text{Payload}^{(\text{single})} \pm 5$ t, $\text{Range}^{(\text{single})} \pm 600$ n mile). Figure 4 shows the mission conditions of three optimizations.

B. Sectional Airfoil Design Optimization

In this section, we introduce a simplified airfoil design optimization problem with 342 operating points based on the previous wing design problem. The optimization objective function is the weighted fuel burn among the 342 missions. We only focus on the influence of the section shape, and we assume the wing sweep angle fixed at

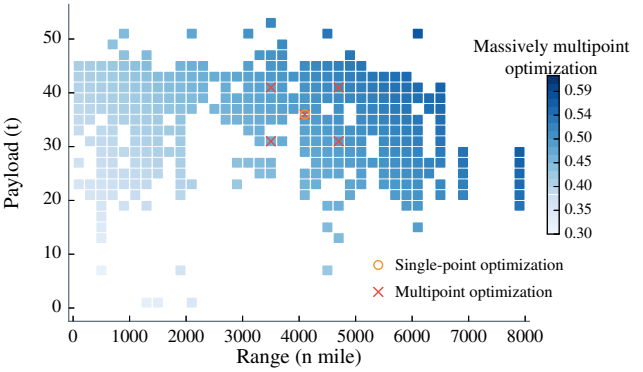

Fig. 4 C_L constraints in the single-point, multipoint, and massively multipoint optimizations of the wing.

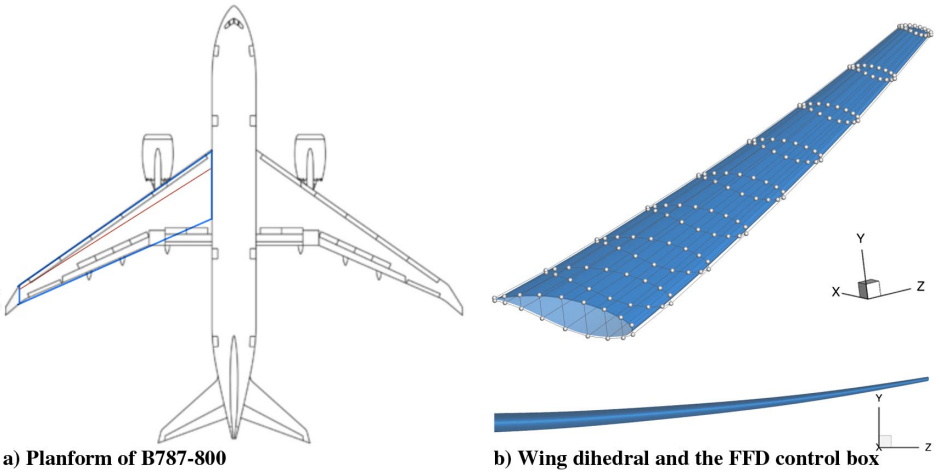

a) Planform of B787-800 **b) Wing dihedral and the FFD control box**

Fig. 3 Baseline wing created using the planform of the B787-800 wing, the dihedral of the CRM wing, and the section shape of the RAE 2822 airfoil.

Table 2 Problem statement of the wing shape optimization for fuel burn reduction in 342 missions

	Functions	Description	Bounds	Quantity
Minimize	$\sum_{i=1}^{342} w^i W_{\text{Fuel}}^i$	Weighted fuel burn	— —	1
With respect to	$\boldsymbol{x}_s$	y perturbation of FFD control points	$c_{\text{local}} \times [-0.01, 0.01]$	162
	Λ	Quarter-chord sweep angle	[22 deg, 42 deg]	1
	α_{twist}	Angles of twist	[−10 deg, 10 deg]	8
	α^i	Angles of attack	[3 deg, 7 deg]	342
Subject to	V	Volume constraint	$[V_{\text{baseline}}, +\infty]$	1
	C_L^i	Lift constraints	$[C_{L,\text{cruise}}^i, C_{L,\text{cruise}}^i]$	342

$\Lambda_{25\%} = 32.2$ deg. Thus, the W_{Wing} is also fixed. Besides, the cruise lift-to-drag ratio C_L/C_D can be $17 \sim 20$ for commercial aircraft. The C_l/C_d for an optimized transonic airfoil could be $65 \sim 80$ [20,45], which is about three times larger. This difference should be bridged to estimate the aircraft fuel burn in the airfoil design optimization, and so we modify Eq. (A3) as follows:

$$W_{\text{Fuel}} = (W_{\text{Payload}} + W_{\text{Wing}} + W_{\text{Rest}})\left(\exp\left(R\frac{g \times \text{SFC}}{V}\frac{C_d}{C_l} \times 4.0\right) - 1\right) \tag{4}$$

where C_l and C_d are the lift and drag coefficients of the sectional airfoil.

Based on industrial practice, we use the following equation to transfer the lift constraints from the wing design to the airfoil design:

$$C_l = \frac{1.1 \times C_L}{\cos^2 \Lambda_{25\%}} \tag{5}$$

Then, the lift constraints of the 342 design points are computed and shown in Fig. 5.

We use the RAE 2822 airfoil as the baseline, which is parameterized using FFD with a 2×10 control box shown in Fig. 6. The y coordinates of the FFD points can move to manipulate the airfoil shape. As in Ref. [3], we have the leading- and trailing-edge points fixed during the optimization by coupling corresponding control points, which leads to 18 independent shape design variables in this problem. In each design point, the operating Mach number is $M = M_{\text{cruise}} \times \cos \Lambda_{25\%} = 0.72$. We allow the angle of attack to vary in [0.0 deg, 5.0 deg] to satisfy C_l constraints. Thickness constraints are added at four positions along the chord ($x/c = 0.2, 0.4, 0.6, 0.8$). The optimization details are shown in Table 3.

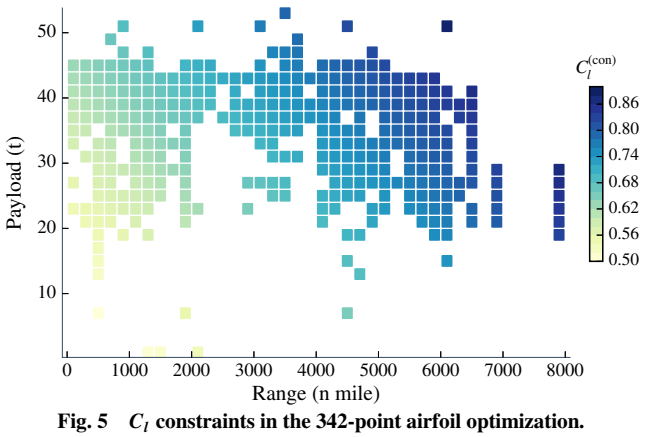

Fig. 5 C_l constraints in the 342-point airfoil optimization.

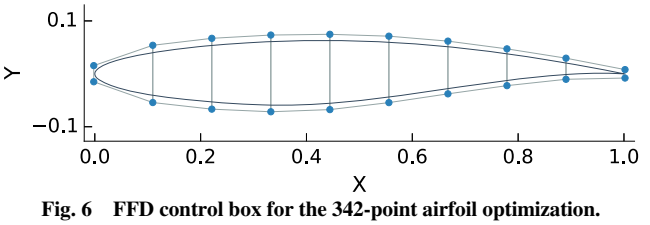

Fig. 6 FFD control box for the 342-point airfoil optimization.

III. Optimization Architecture for Massively Multipoint Aerodynamic Design

We present our optimization method for massively multipoint aerodynamic design problems in Sec. III.A. Next, we introduce the supportive algorithms for the optimization method in Secs. III.B–III.D.

A. Surrogate-Assisted Gradient-Based Optimization Method

In massively multipoint design optimization, the objective function f is a weighted combination of performance among all design points. We note the shape design variables and flow condition variables as $\boldsymbol{x}_s$ and $\boldsymbol{x}_f$, respectively. Then, we have

$$f(\boldsymbol{x}_s, \boldsymbol{x}_f^1, \ldots, \boldsymbol{x}_f^{N_{\text{mission}}}) = \sum_{i=1}^{N_{\text{mission}}} w^i f^i(\boldsymbol{x}_s, \boldsymbol{x}_f^i) \tag{6}$$

where N_{mission} is the number of design points, and w^i is the ith combination coefficient. In most cases, only the angles of attack $(\alpha^1, \ldots, \alpha^{N_{\text{mission}}})$ are to be determined via the optimization, whereas other variables in $\boldsymbol{x}_f$ like Mach numbers $(M^1, \ldots, M^{N_{\text{mission}}})$ are predetermined. Without loss of generality, the optimization problem can be written as

$$\begin{aligned} &\text{Minimize} && f(\boldsymbol{x}_s, \boldsymbol{x}_f^1, \ldots, \boldsymbol{x}_f^{N_{\text{mission}}}) \\ &\text{with respect to} && \boldsymbol{x}_s, \alpha^1, \ldots, \alpha^{N_{\text{mission}}} \\ &\text{subject to} && f_a^1(\boldsymbol{x}_s, \boldsymbol{x}_f^1) \le 0.0 \\ & && \vdots \\ & && f_a^{N_{\text{mission}}}(\boldsymbol{x}_s, \boldsymbol{x}_f^{N_{\text{mission}}}) \le 0.0 \\ & && g(\boldsymbol{x}_s) \le 0.0 \end{aligned} \tag{7}$$

where f_a^i, $i = 1, \ldots, N_{\text{mission}}$, is the aerodynamic constraint of each design point; and g represents geometric constraints on the aerodynamic shape. Both constraints can also be equality ones based on specific demand.

The high dimensionality in this problem is typically due to shape design variables. In each optimization iteration, different design points are only diverse in a low-dimensional space spanned by flow condition variables. To efficiently solve massively multipoint aerodynamic shape optimization problems, we propose a two-loop optimization method shown in Fig. 7. The outer loop of this method is controlled by a gradient-based optimization algorithm, which efficiently searches the high-dimensional design space. The inner loop contains an infill sampling process to construct and refine surrogate models in the low-dimensional $\boldsymbol{x}_f$ space. These surrogate models

Table 3 Problem statement of the 342-point airfoil optimization

	Functions	Description	Bounds	Quantity
Minimize	$\sum_{i=1}^{342} w^i W^i_{\text{Fuel}}$	Weighted fuel burn	— —	1
With respect to	$\boldsymbol{x}_s$	y perturbation of FFD control points	$[-0.01, 0.01]$	18
	α^i	Angles of attack	[0 deg, 5 deg]	342
Subject to	t	Thickness constraints	$[0.9t_{\text{baseline}}, +\infty]$	4
	C_l^i	Lift constraints	$[C_l^{(i,\text{con})}, C_l^{(i,\text{con})}]$	342

provide fast approximations of objective functions, constraint functions, and their gradients to all design variables. Therefore, this method takes advantages from both the high efficiency of the gradient-based optimization and the low computational cost of surrogate models without suffering from the curse of dimensionality.

We use pyOptSparse [46,47] as the gradient-based optimization framework and adopt the sequential least-squares programming (SLSQP) algorithm implemented in pyOptSparse as the gradient-based optimizer. In each gradient-based optimization iteration, we first sample the $\boldsymbol{x}_f$ space using the Latin hypercube sampling (LHS) method. For the fuel burn reduction problem in this paper, $\boldsymbol{x}_f$ only contains α, and so it just spans a one-dimensional space. To maintain the versatility of solving multidimensional problems, we use LHS, although it is not more advantageous than other sampling methods in the one-dimensional problem. Then, we add new sampling points based on the estimated error that will be introduced in Algorithm 1. These samples are evaluated by an in-house CFD code called Exstream with Reynolds-averaged Navier–Stokes and adjoint solvers [10,48]. F in Fig. 7 represents both the objective function and aerodynamic constraint functions. GEK [49,50] is used to predict F because gradients with respect to $\boldsymbol{x}_f$ are available in the training data. GEK models are also used to provide approximations of gradients to flow condition variables ($\mathrm{d}F/\mathrm{d}\boldsymbol{x}_f$) using the finite difference method. POD kriging is used to predict gradients to shape design variables ($\mathrm{d}F/\mathrm{d}\boldsymbol{x}_s$).

The inner loop is a refining process by adding new samples, and each sample is chosen by solving a suboptimization problem. To reduce the possibility of being stuck to local optima, we use a gradient-free algorithm: particle swarm optimization implemented in pyswarm [51]. It performs well when the dimension of the problem is low.

B. Kriging with POD for Multiple Outputs

Surrogate models [52] provide low-cost substitutes to costly functions. Among different surrogates, kriging [50,53,54] is a popular choice in aerodynamic design optimization [3,22,55]. One advantage over other surrogate models is that kriging provides the prediction variance, which is instructive to add new sampling points. The efficient global optimization (EGO) method [56] leverages the variance function of kriging to significantly improves the efficiency of surrogate-based optimization [3,22].

For a function with input $\boldsymbol{x} \in \mathbb{R}^n$ and a scatter output y, based on the derivation of previous research [54,55], the output prediction using an ordinary kriging model can be expressed as

$$\hat{y}(\boldsymbol{x}) = \hat{\beta}_0 + \boldsymbol{r}^T R^{-1}(\boldsymbol{y}_s - \mathbf{1}\hat{\beta}_0) \tag{8}$$

where $\boldsymbol{y}_s = (y^{(1)}, y^{(2)}, \ldots, y^{(n_s)})^T$ is the vector of observed outputs on input points $\boldsymbol{x}^{(1)}, \boldsymbol{x}^{(2)}, \ldots, \boldsymbol{x}^{(n_s)}$; $\hat{\beta}_0 = (\mathbf{1}R^{-1}\mathbf{1})^{-1}R^{-1}\boldsymbol{y}_s$; and $\mathbf{1} \in \mathbb{R}^{n_s}$ is a column vector for which the elements are all filled with ones. $R \coloneqq [R(\boldsymbol{x}^{(i)}, \boldsymbol{x}^{(j)})]_{ij} \in \mathbb{R}^{n_s \times n_s}$, and $\boldsymbol{r}(\boldsymbol{x}) \coloneqq [R(\boldsymbol{x}^{(i)}, \boldsymbol{x})]_i \in \mathbb{R}^{n_s}$. $R(\boldsymbol{x}, \boldsymbol{x}')$ is the kernel of the kriging model, which is a spatial function of $\boldsymbol{x}$ and $\boldsymbol{x}'$ that depends on the distance between them. The performance of kriging models is influenced by the kernel used, but this discussion is beyond the scope of this paper. We use the popular Gaussian exponential correlation function as the kernel:

$$R(\boldsymbol{x}, \boldsymbol{x}') = \prod_{i=1}^{n} \exp(-\theta_i (x_i - x_i')^2), \quad \forall\ \theta_i \in \mathbb{R}^+ \tag{9}$$

Besides, kriging provides the mean squared error $s^2(\boldsymbol{x})$ of the prediction, which indicates the uncertainty of the prediction:

$$s^2(\boldsymbol{x}) = \hat{\sigma}^2[1 - \boldsymbol{r}^T R^{-1}\boldsymbol{r} + (1 - \mathbf{1}R^{-1}\boldsymbol{r})^2/(\mathbf{1}^T R\mathbf{1})] \tag{10}$$

where $\hat{\sigma}^2 = (\boldsymbol{y}_s - \mathbf{1}\hat{\beta}_0)^T R^{-1}(\boldsymbol{y}_s - \mathbf{1}\hat{\beta}_0)/n_s$.

Training the model leads to an optimization of hyperparameters θ_i ($i = 1, \ldots, n$) in Eq. (9), which is performed to maximize the likelihood function $\tilde{L}$:

$$\tilde{L} = \frac{1}{\sqrt{(2\pi\hat{\sigma}^2)^{n_s}|R|}} \exp\left(-\frac{1}{2}\frac{(\boldsymbol{y}_s - \hat{\beta}_0\mathbf{1})^T R^{-1}(y_s - \hat{\beta}_0\mathbf{1})}{\hat{\sigma}^2}\right) \tag{11}$$

This function is highly multimodal [57], and so gradient-free optimization algorithms like the genetic algorithm and particle swarm optimization are more suitable. This optimization takes the majority of computational cost in kriging construction.

As shown in Eq. (11), different output functions lead to different hyperparameter optimizations, and so the computational cost

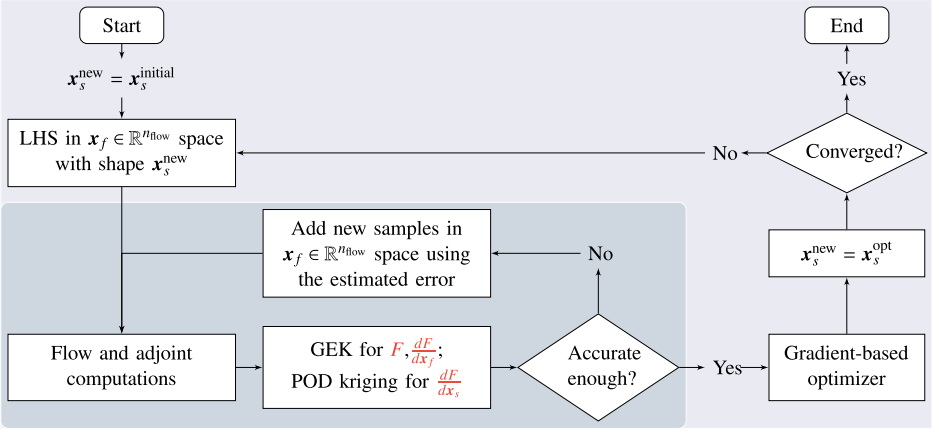

Fig. 7 Flowchart of the surrogate-assisted gradient-based optimization method.

increases with the number of outputs. In aerodynamic shape optimization, the number of design variables can be several hundred, whereas the concerned aerodynamic functions mainly include the coefficients of drag, lift, and moments. It is more challenging to predict hundreds of gradient functions than just several aerodynamic functions. Besides, gradients may be more nonlinear than aerodynamic functions, and so it would be more costly to construct accurate surrogate models for them. We introduce a POD-kriging method [58–61] to reduce the construction cost of surrogate models for multiple outputs. To accelerate the training process, POD kriging reduces the number of outputs by projecting them to a low-dimensional subspace, where the outputs $\boldsymbol{y} \in \mathbb{R}^m$ are expressed as

$$\boldsymbol{y} \approx \boldsymbol{\Phi c} + \bar{\boldsymbol{y}} \tag{12}$$

and $\bar{\boldsymbol{y}} \in \mathbb{R}^m$ is a constant vector presenting the mean of $\boldsymbol{y}$ in the original space. $\boldsymbol{\Phi} \in \mathbb{R}^{m\times l}$ is the basis of the lower-dimensional subspace, and $\boldsymbol{c} \in \mathbb{R}^l$ is a combination of coefficients. With this projection, we only need to construct surrogate models for the basis coefficients $\boldsymbol{c}$ instead of the outputs $\boldsymbol{y}$. Because $l < m$, this approach reduces the training cost in problems with multiple outputs, such as high-dimensional aerodynamic gradients.

The selection of the low-dimensional subspace should make the projection introduce the smallest error. This means that output vectors $\boldsymbol{y}^{(i)}$, $i = 1, \ldots, n_s$, have the largest projection on the selected subspace:

$$\boldsymbol{\Phi} = \max_{\boldsymbol{\Psi}} \frac{1}{n_s} \sum_{i=1}^{n_s} \|(\boldsymbol{y}^{(i)}, \boldsymbol{\Psi})\| \tag{13}$$

We use the snapshot POD to determine the subspace satisfying Eq. (13). First, we have $\bar{\boldsymbol{y}} = (\boldsymbol{y}^{(1)} + \cdots + \boldsymbol{y}^{(n_s)})/n_s$, and the snapshot matrix $\boldsymbol{C}$ is constructed as

$$\boldsymbol{C} = [\boldsymbol{y}^{(1)} - \bar{\boldsymbol{y}}, \boldsymbol{y}^{(2)} - \bar{\boldsymbol{y}}, \ldots, \boldsymbol{y}^{(n_s)} - \bar{\boldsymbol{y}}] \tag{14}$$

Then, perform a singular value decomposition on $\boldsymbol{C}$:

$$\boldsymbol{C} = \boldsymbol{U\Sigma V}^T \tag{15}$$

where $\boldsymbol{U}$ contains the basis of the selected subspace. The diagonal entries in $\boldsymbol{\Sigma}$ (the singular values of $\boldsymbol{A}$) are sorted in descending order. The columns in $\boldsymbol{U}$ are corresponding to singular values from largest to smallest, which means they are sorted by the importance. We refer to the ith column in $\boldsymbol{U}$ as POD mode i.

Figure 8 shows the POD modes for gradients of C_l and C_d in the airfoil design case introduced in Sec. II.B. We compute these modes using 100 samples that have the same airfoil shape but differ in the flow condition: α. Figure 9 shows that the first several POD modes

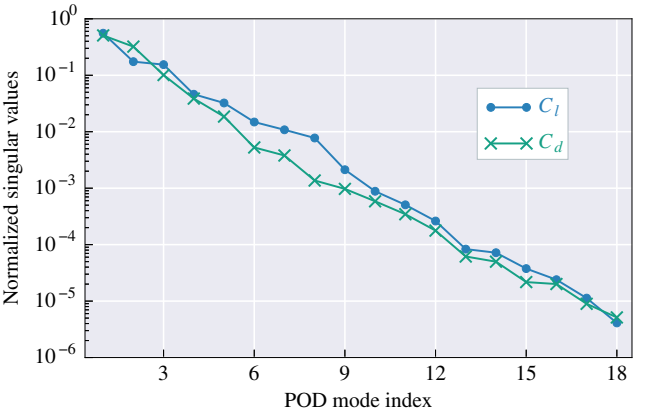

Fig. 9 Singular value decay of C_l and C_d gradients.

dominate the energy in the output space. For example, the first nine POD modes of C_d gradients take more than 99% of the energy. Nevertheless, the truncation of POD modes still introduces a projection error. We use ε to quantify this error:

$$\varepsilon = \sum_{i=1}^{n_{\text{test}}} \frac{\|\boldsymbol{z}^{(i)} - \boldsymbol{y}^{(i)}\|_2}{n_{\text{test}} \times \|\boldsymbol{y}^{(i)}\|_2} \tag{16}$$

where $\boldsymbol{z}$ is the approximation of the output $\boldsymbol{y}$ by POD kriging. Figure 10 shows that projection error calculated by Eq. (16) with $n_{\text{test}} = 500$, and it has a similar tendency with the singular value decay in Fig. 9. The projection error magnitude is reduced by increasing the number of POD modes. In this case, using all POD modes with normalized singular values above 0.01 approximately makes the projection error within 0.01.

We further compare the accuracy of POD kriging and kriging in predicting gradients of aerodynamic coefficients. To reduce the influence of the design of experiments (DOE), we conduct multiple tests and use LHS to generate training samples in the space spanned by the flow condition variable. The validation data are composed of 500 samples evenly distributed in the same space. The relative error is computed by Eq. (16), where $\boldsymbol{z}$ is the gradient predicted by surrogate models. Nine modes are used in POD kriging, and its training cost is only half of the training cost of kriging in this case. This advantage is more significant in higher-dimensional problems such as wing shape optimization. As shown in Fig. 11, POD kriging is as accurate as kriging, in spite of the projection error.

The result shown in Fig. 11 seems to be unreasonable because there is a projection error in POD kriging. To further investigate this phenomenon, we conduct a series of tests to show the error of POD kriging with a different number of POD modes. Figure 12 shows the

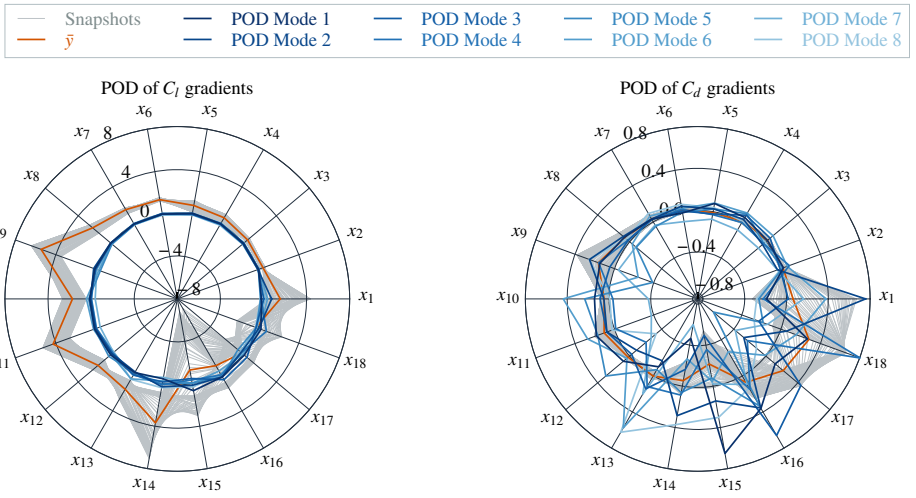

Fig. 8 POD modes for gradients of C_l and C_d to 18 airfoil shape variables.

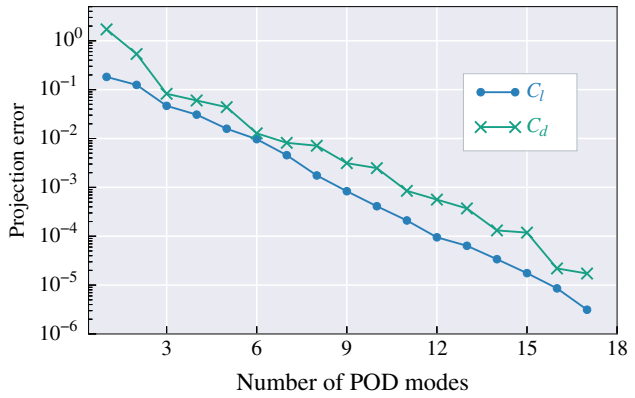

Fig. 10 Projection error of C_l and C_d gradients using different numbers of modes.

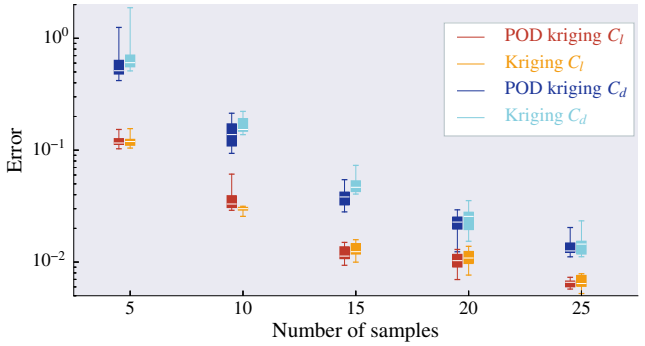

Fig. 11 POD kriging can be as accurate as kriging in predicting gradients of C_l and C_d.

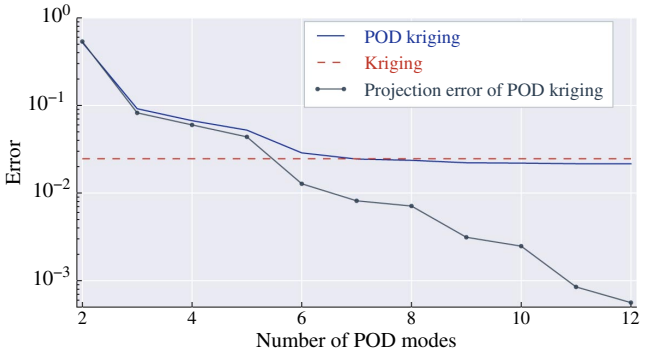

Fig. 12 POD kriging is as accurate as kriging when the projection error is insignificant.

average relative error of C_d gradients with surrogate models trained by 20 samples. It can be seen that the error of POD kriging is mainly due to the projection error when insufficient POD modes are used (less than six). POD kriging is less accurate than kriging in this situation. However, POD kriging turns to be a bit more accurate when the projection error becomes insignificant with more POD modes used. Although the accuracy of kriging seems to be the ceiling for POD kriging, the training cost of POD kriging is much lower. We adopt this approach to predict gradients of the aerodynamic coefficient to shape design variables.

C. Adaptive Sampling Method Based on the Estimated Error

Several criteria for adding new samples exist in the literature [56,62–64]. The expected improvement (EI) criterion used in EGO [56] is a popular one. It is designed to improve the surrogate model's accuracy around the potential optimum so that the surrogate-based optimization could converge efficiently. Nevertheless, the EI criterion is not the most efficient approach to improving the overall accuracy, which is a requirement in this work. Another criterion, called the maximum variance [62], uses the mean squared error s^2 as an approximation of the prediction error to add new samples. However, s^2 differs much from the real error (Fig. 13). This is because s^2 is mostly related to the position of inputs but has no direct relationship to the output function.

To have a better estimation of the prediction error, we use the leave-one-out strategy to construct a function, which is referred to as the estimated error. The construction process of this error is detailed in Algorithm 1. For a kriging model f_{ori} trained by n_s samples, we gradually train a series of kriging models f_i using the leave-one-out strategy. The changes of prediction $|f_{\text{ori}} - f_i|$ on a dense set of sampling points $\boldsymbol{x}_{\text{dense}}$ are recorded and summed up as $\boldsymbol{\delta}$. This leave-one-out change of prediction could represent the error tendency of f_{ori}. Then, we train a surrogate model f_δ to predict this change and construct the estimated error using $f_\delta \times s^2$. This formula is a combination of kriging uncertainty and error tendency. Figure 13 shows the comparison of s^2 and the estimated error in three algebraic cases with different complexities, where the kriging models are trained by five samples evenly distributed in $[-2.0, 2.0]$. It can be seen that s^2 cannot capture the tendency of the real prediction error, whereas maximizing the estimated error computed by Algorithm 1 leads to a point close to the real maximal error point.

Based on the previous analysis, adding samples using the estimated error can be more beneficial than s^2. We compare their performance in the airfoil optimization problem, where the surrogate model is used to predict POD mode coefficients of C_l gradients to 18 shape design variables. The prediction error is computed using

$$\text{Error} = \frac{\|\boldsymbol{y}^{\text{kriging}} - \boldsymbol{y}^{\text{CFD}}\|_2}{\|\boldsymbol{y}^{\text{CFD}}\|_2} \tag{17}$$

where $\boldsymbol{y}^{\text{kriging}}$ and $\boldsymbol{y}^{\text{CFD}}$ are the coefficients of 500 validation samples computed by the surrogate model and CFD, respectively. As a

Algorithm 1: Estimated error with the leave-one-out strategy

procedure: ESTERROR ($f_{\text{ori}}, \boldsymbol{x}, \boldsymbol{x}^1, \ldots, \boldsymbol{x}^{n_s}, y^1, \ldots, y^{n_s}$) ▷ Compute the estimated error of f_{ori} at $\boldsymbol{x}$.
  $\boldsymbol{x}_{\text{dense}} \leftarrow$ A vector of sampling points infilling the design space densely
  for $i = 1; i \le n_s; i++$, **do** ▷ Cycle all training points
    $f_i \leftarrow$ Construct a surrogate model using all training points except the ith one
    $\boldsymbol{y}_{\text{ori}} = f_{\text{ori}}(\boldsymbol{x}_{\text{dense}})$
    $\boldsymbol{y}_{\text{new}} = f_i(\boldsymbol{x}_{\text{dense}})$
    $\boldsymbol{\delta} += |\boldsymbol{y}_{\text{ori}} - \boldsymbol{y}_{\text{new}}|$ ▷ Record and sum up changes in the prediction
  end for
  $f_\delta \leftarrow$ Train a surrogate model of the total changes using $(\boldsymbol{x}_{\text{dense}}, \boldsymbol{\delta})$
  $f_{\text{EstError}}(\boldsymbol{x}) = f_\delta(\boldsymbol{x}) \times s^2(\boldsymbol{x})$ ▷ Modify the estimation with the mean squared error s^2 provided by f_{ori}
  return $f_{\text{EstError}}(\boldsymbol{x})$ ▷ Return the estimated error at $\boldsymbol{x}$
end procedure

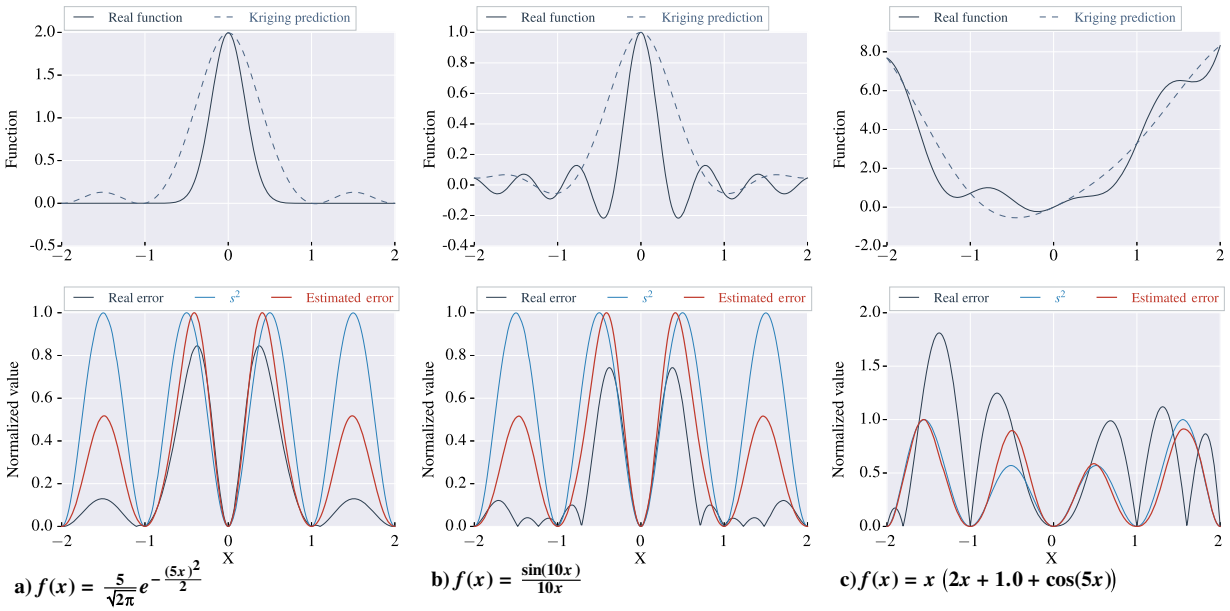

Fig. 13 Comparison of the estimated error and s^2 in three algebraic functions.

comparison, we also conduct tests that only use LHS to generate samples in each sampling step. To reduce the influence from the DOE, we conduct 10 different tests and show the mean error and error distributions using lines and intervals, respectively. As shown in Fig. 14, adding samples based on either s^2 or the estimated error is better than using LHS, and the estimated error is the most efficient approach to improving surrogate model accuracy. The advantage of the estimated error is more obvious in the prediction of the second POD mode coefficient, where an accurate surrogate model is more difficult to construct. We use the adaptive sampling criterion based on the estimated error to refine surrogate models in the following content.

D. Termination Criterion of the Infill Sampling Process

The refinement of surrogate models by adding more samples is critical to the optimization. If surrogate models are inaccurate, the optimization may converge to undesired solutions or even fail to converge. However, excessive refinement calls for too many CFD and adjoint evaluations, which decreases overall optimization

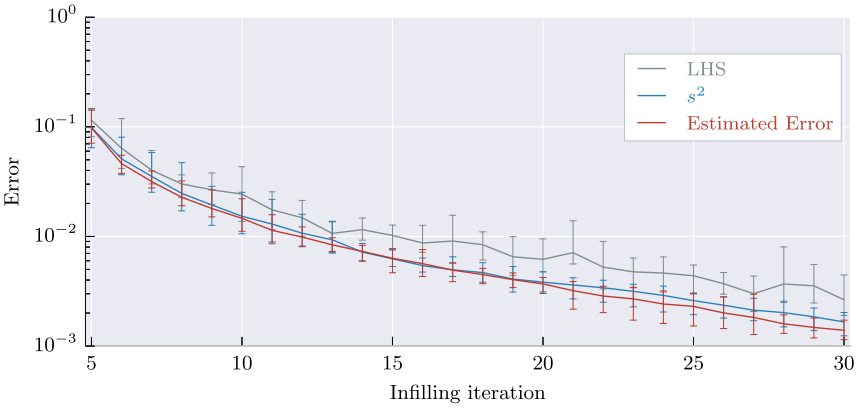

a) The first POD mode coefficient of C_l gradients

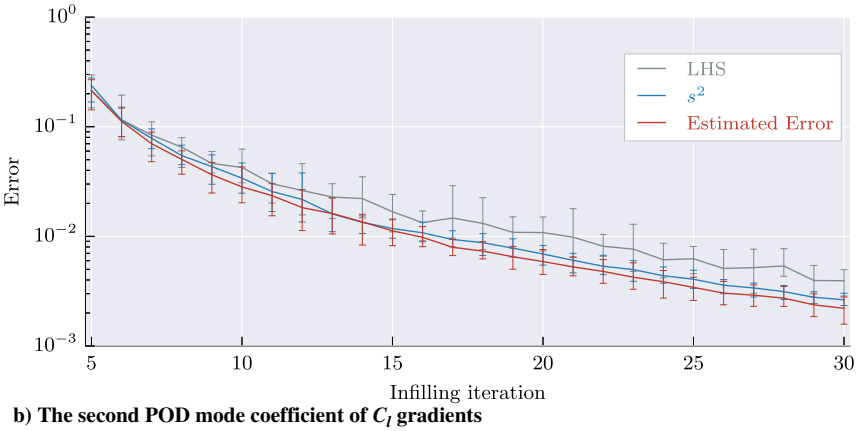

b) The second POD mode coefficient of C_l gradients

Fig. 14 Prediction error decreasing the fastest when new samples are added based on the estimated error.

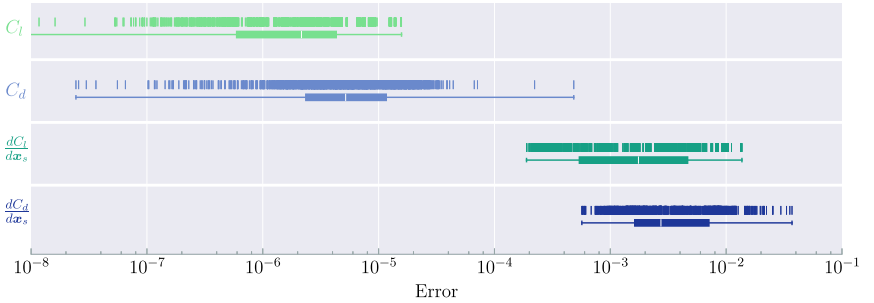

Fig. 15 Relative error of aerodynamic functions and gradients evaluated by surrogate models.

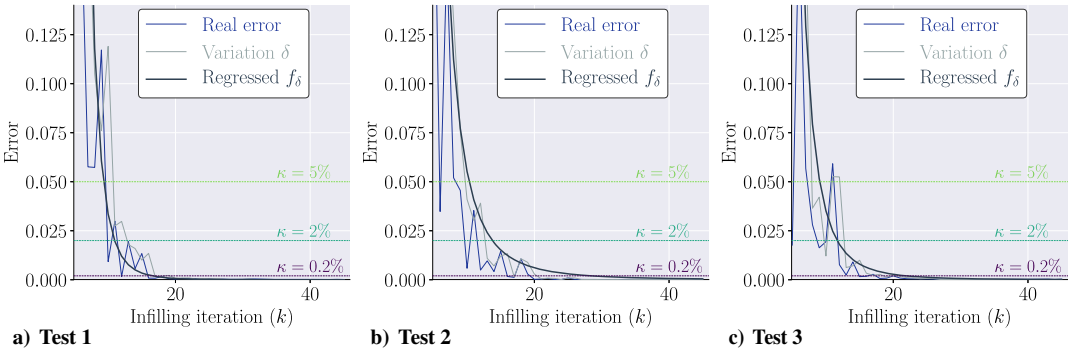

Fig. 16 Termination of the infill sampling process with different thresholds.

efficiency. So, the termination criterion of the infill sampling process could influence the optimization.

In the inner loop of the proposed massively multipoint optimization method, surrogate models for C_l, C_d, and their gradients are constructed. Among different aerodynamic coefficients, the profile of C_d is the most complex; and the surrogate model of this function is usually the most inaccurate [20]. Figure 15 shows relative errors in the evaluation of aerodynamic coefficients and gradients, where we use 30 and 100 LHS points to train and validate these models, respectively. We conduct 10 different tests to reduce the influence of the DOE. Errors in Fig. 15 are shown with scatter plots and corresponding box plots. The scatter plot provides the error of each validating point, and the box plot provides the statistics for these errors. The white line in the box plot indicates the median of these errors. Because the largest error exists in the prediction of C_d gradients ($\mathrm{d}C_d/\mathrm{d}\boldsymbol{x}_s$), we add samples via maximizing the estimated error of C_d gradients in the inner loop of the optimization. This criterion not only reduces the error of $\mathrm{d}C_d/\mathrm{d}\boldsymbol{x}_s$ but also improves the accuracy of other surrogate models.

The termination of the infill sampling process should be based on the error of surrogate models. Because the real error is not available in the infill sampling process, we use the variation in the prediction of the weighted $\mathrm{d}C_d/\mathrm{d}\boldsymbol{x}_s$ as the sign of error. With surrogate models becoming more accurate, the variation of the predictions between different steps is getting smaller, and so it could play the role of an "observed error." We note the variation in the kth ($k \geq n_{\mathrm{LHS}} + 1$) infill sampling step as $\delta^{(k)}$, which is computed by

$$\delta^{(k)} = \frac{\|(\mathrm{d}C_d/\mathrm{d}\boldsymbol{x}_s)^{(k)}_{\mathrm{weighted}} - (\mathrm{d}C_d/\mathrm{d}\boldsymbol{x}_s)^{(k-1)}_{\mathrm{weighted}}\|}{\|(\mathrm{d}C_d/\mathrm{d}\boldsymbol{x}_s)^{(k)}_{\mathrm{weighted}}\|} \tag{18}$$

We conduct several tests to investigate the difference between the real error and variation. Figure 16 shows their decays with the increase of the number of samples. It can be seen that δ and the real error vary a bit, despite them having similar trends. The δ decay lines especially fluctuate too much. Thus, using δ directly to terminate the infill sampling process might be problematic. To obviate the influence of fluctuations, we regress a power function f_δ based on δ:

$$f_\delta(k) = (ak + b)^c \tag{19}$$

where a, b, and c are the regression parameters. The index value $c < 0$, so that f_δ could capture the decreasing character of δ. Also, a scales the base value in f_δ, and b translates it. A natural regression can be achieved by optimization of a, b, and c.

We use Eq. (19) to perform regressions because of its downward trend of approaching zero, which could smoothly capture the decreasing δ. As shown in Fig. 16, the regressed f_δ curves reasonably indicate the decay of prediction errors. With $f_\delta \leq \kappa$ as the termination criterion, the infill sampling process can be terminated automatically. Figure 16 also shows the termination iterations identified by $\kappa = 5\%$, $\kappa = 2\%$, and $\kappa = 0.2\%$. Actually, the indication can be regressed by using other functions: for example, the index function $f_\delta(k) = c^{(ak+b)}$ with $0.0 < c < 1.0$. Further study on regression functions is beyond the scope of the present paper and is left to future work.

IV. Optimization Results Analysis

One possible issue of the proposed optimization architecture is the nonconvergence due to the approximation in the gradients provided by surrogate models. These surrogate models are trained by adaptive samples and would lead to nonsmoothness of the objective and constraint functions as seen by the outer-loop optimizer. We address this problem by using a conservative inner-loop termination threshold. We investigate its influence in Sec. IV.A by performing massively multipoint airfoil design optimizations with different thresholds. Then, we perform the wing shape optimization in Sec. IV.B and compare the results with regular single-point and multipoint optimization.

A. Sectional Airfoil Design Optimization

We first investigate the proposed optimization method in the airfoil design optimization case. As discussed previously, we use the regressed $f_\delta \leq \kappa$ to terminate each inner loop in the massively multipoint optimization. Note that κ is referred to as the termination threshold. Figure 17 shows the convergence histories of three optimizations with $\kappa = 5\%$, $\kappa = 2\%$, and $\kappa = 0.2\%$. Inaccurate

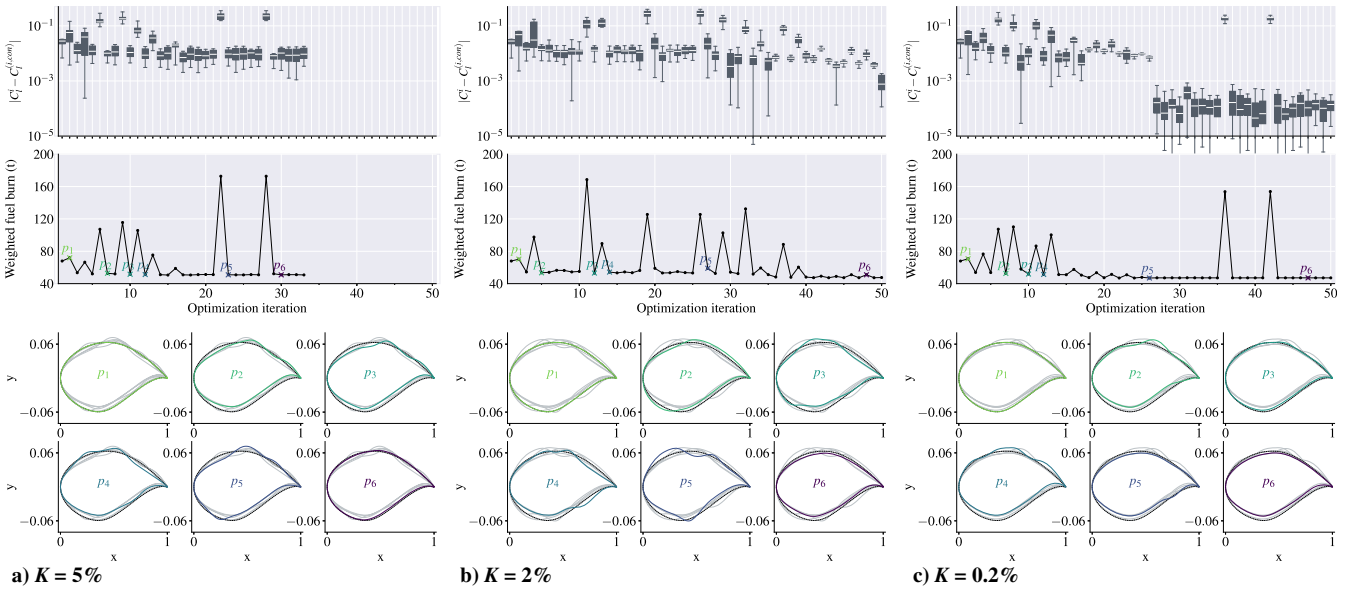

a) $K = 5\%$ b) $K = 2\%$ c) $K = 0.2\%$

Fig. 17 The 342-point airfoil optimization with different termination thresholds in the infill sampling process.

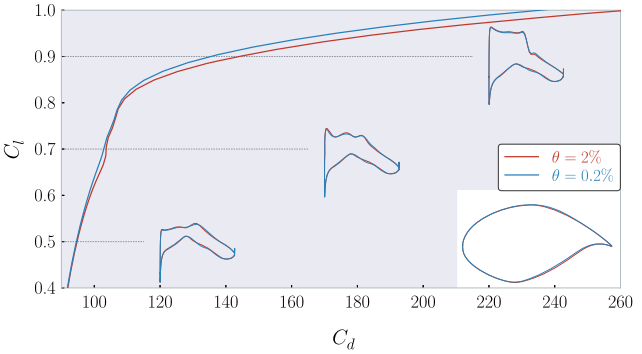

Fig. 18 Drag polar curves of airfoils optimized with different termination thresholds in the infill sampling process.

gradients with the loose threshold ($\kappa = 5\%$) make the optimization (Fig. 17a) fail to converge. Although further shrinking the airfoil thickness does not violate the thickness constraints and could reduce the fuel burn by decreasing the drag, the optimization just stops early at an airfoil shape close to the baseline after several searches in the design space. Using more accurate gradients with $\kappa = 2\%$ makes the optimization converge to a smooth airfoil shape lying close to the lower thickness constraint bounds (Fig. 17b). However, the lift constraints on different design points are not well satisfied. A conservative threshold with $\kappa = 0.2\%$ leads to faster convergence, and all constraints are satisfied in the end (Fig. 17c). Generally, using more conservative thresholds leads to more accurate gradient approximations and helps to make the optimization converge, but loose thresholds would result in early optimization termination. A conservative threshold ensures the convergence of the outer loop, which determines the success or failure of the optimization.

We allow a maximum of 50 SLSQP iterations, including the line searching. The computational costs of massively multipoint optimization with $\kappa = 2\%$ and $\kappa = 0.2\%$ are 624 and 1223 CFD evaluations. The average numbers of samples used to train surrogate models with $\kappa = 2\%$ and $\kappa = 0.2\%$ are 12.5 and 24.5, respectively. The construction cost of surrogate models is mainly due to CFD and adjoint evaluations of these samples, and then estimations with surrogate models are done almost in real time. The ratio of surrogate construction to estimation (offline-to-online cost ratio) could be over 100,000, which is rather high. Nevertheless, the total cost of the massively multipoint optimization is only several times the regular single-point or multipoint optimization.

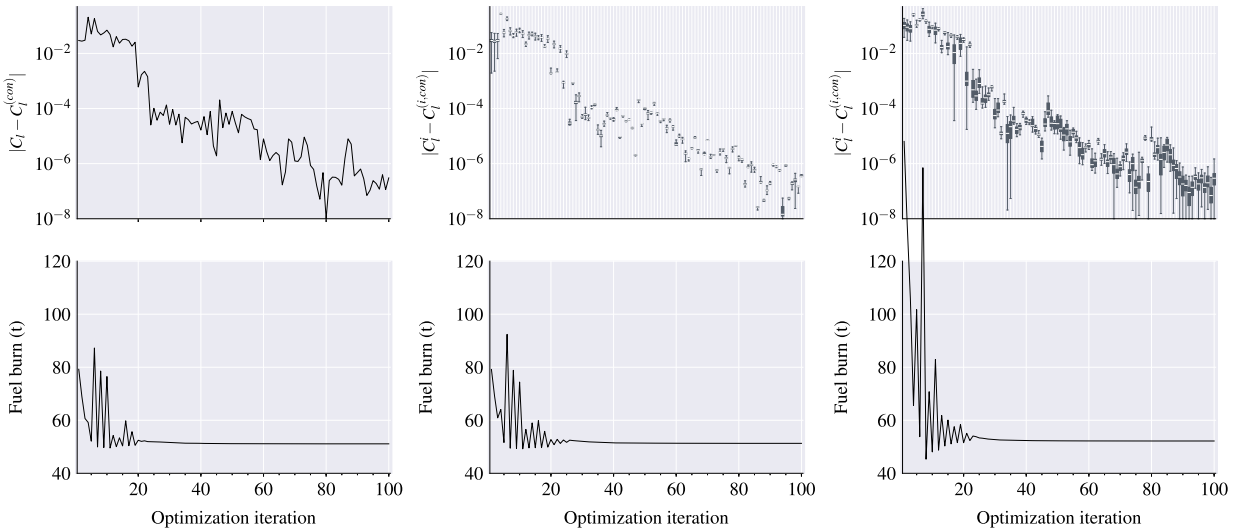

a) Single-point optimization b) Multipoint optimization c) Massively multipoint optimization

Fig. 19 Massively multipoint optimization of the wing has a similar convergence history with the regular single-point and multipoint optimizations.

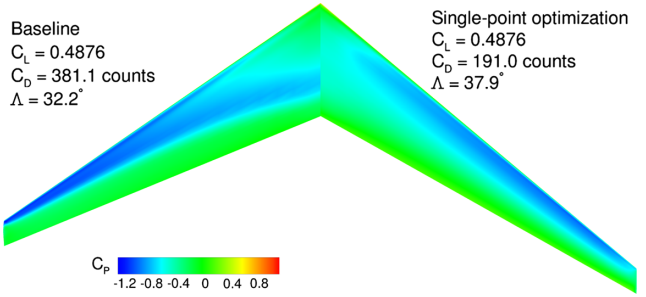

Fig. 20 Single-point optimization significantly improves the aerodynamic performance of the baseline wing.

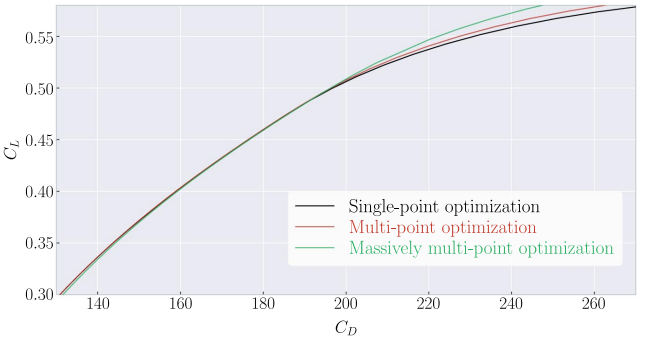

Fig. 22 Massively multipoint optimal design produces the smallest drag when a large cruise lift is required.

Figure 18 shows drag polar curves of airfoils optimized with $\kappa = 2\%$ and $\kappa = 0.2\%$. Although the optimized airfoil shapes and C_p distributions are similar, the optimal design with $\kappa = 0.2\%$ has a wider polar curve. Thus, it produces a smaller drag to generate a certain lift: especially when $C_l > 0.82$. With an accurate evaluation, we find that the weighted fuel burns of optimized airfoils with $\kappa = 2\%$ and $\kappa = 0.2\%$ are reduced to 47,463 and 47,137 kg, respectively. Optimization with $\kappa = 0.2\%$ reduces the fuel burn by 326 kg more than the optimization with $\kappa = 2\%$ at the cost of double computational time. So, using a moderate threshold in the early design stage could reduce the computational cost. A conservative threshold should be used in the detail design phase to achieve more fuel burn reduction.

Based on the results of this case, we find that the proposed method may fail to converge when a loose threshold κ is used in the infill sampling termination criterion. Decreasing κ improves the optimization robustness. Therefore, in order to obtain reliable optimization results, a conservative threshold should be used. We would recommend using κ around 1%, or even smaller in similar cases.

B. Wing Shape Design Optimization

We apply the proposed massively multipoint optimization method in the wing shape optimization problem to reduce the total fuel burn. A single-point optimization and regular multipoint optimization are also performed as comparisons. Figure 19 shows their convergence histories. We allow 100 evaluations of the objective function in each optimization. Lift constraints are all well satisfied at the end of each case. In the massively multipoint optimization, we use a termination threshold of $\kappa = 0.5\%$ based on the previous discussions, and the convergence is not more difficult than that in the single-point or multipoint optimization.

Because the baseline wing is given without design optimization, it consumes a huge amount of fuel burn: 100,633.4 kg average among 342 flight missions. Figure 20 shows the optimal design of single-point optimization. The design reduces shock waves and produces a much smaller drag coefficient than the baseline, which improves the aerodynamic performance of the ondesign point. The single-point optimal design has the weighted fuel burn reduced to 52,222.2 kg. The designs of the multipoint optimization and massively multipoint optimization are shown in Fig. 21, and they improve the single-point optimal design mainly by changing the sweep angle. The weighted fuel burn is further reduced to 52,086.3 and 51,962.9 kg by the multipoint optimization and massively multipoint optimization, respectively. With the single-point optimal design as the reference baseline, the multipoint optimal design and massively multipoint optimal design achieve 0.26 and 0.50% more reductions in fuel burn.

Aircraft design is based on trading off performances among different flight missions, and so it is critical to select suitable ondesign points. As shown in Fig. 4, the single-point optimization and multipoint optimization only consider flight missions with moderate ranges and payloads, where lift coefficients smaller than 0.5 are generally required. The massively multipoint optimization involves flight missions associated with larger cruise lift coefficients. As a result, the massively multipoint optimal design produces much smaller drags than the other two designs when $C_L > 0.5$, which is shown in Fig. 22. The drawback of this design is that it produces larger drags in the domain with $C_L < 0.35$. However, based on the flight missions in Figs. 2 and 4, this aircraft would rarely be operated in missions with such small lift coefficients. Figure 23 shows that this design consequently achieves more fuel burn reductions in missions with longer ranges and larger payloads. The reduction in fuel burn can be as much as 4000 kg in several missions. The design of multipoint optimization has a slightly higher efficiency in the opposite domain, where the flight ranges and payloads are small. A thorough trading off among all flight missions makes the massively multipoint optimal design in line with the actual demand.

In this case, the average number of samples among different iterations in the massively multipoint optimization is 26. However, this number should be 342 if a gradient-based method is directly used to solve this problem. The proposed optimization method reduces the computational cost of direct gradient-based optimization by more than one order, which provides an efficient approach to a more comprehensive consideration of the actual demand.

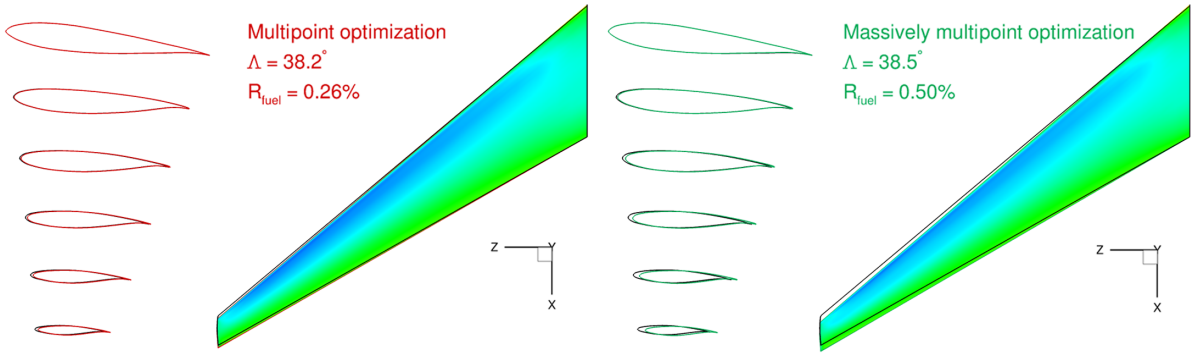

a) Multipoint optimization reduces the fuel burn of the single-point optimal design by 0.26%

b) Massively multipoint optimization reduces the fuel burn of the singlepoint optimal design by 0.50%

Fig. 21 Massively multipoint optimization achieves a larger fuel burn reduction.

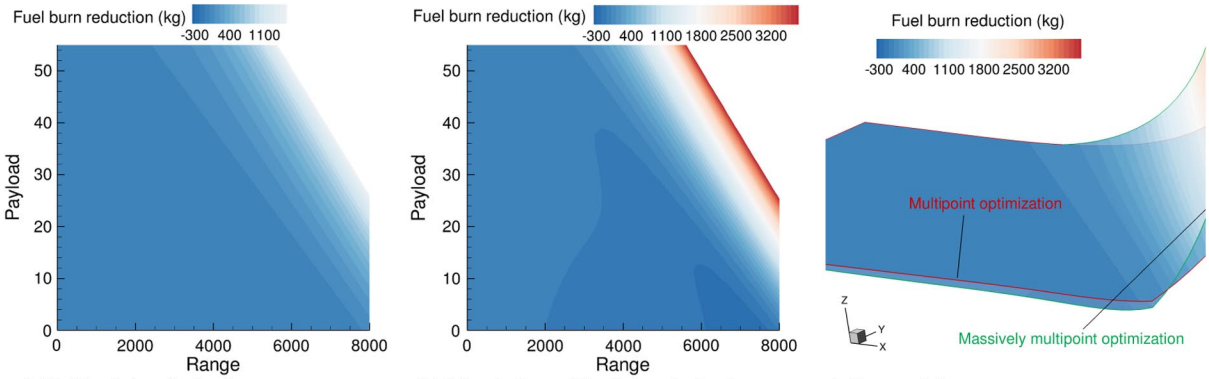

a) Multipoint optimization **b) Massively multipoint optimization** **c) Comparision**

Fig. 23 Fuel burn reduction by the multipoint and massively multipoint optimaldesigns.

The regular multipoint optimization only reduces the fuel burn of the single-point optimal design by 0.26%, which is slight in comparison to the result (about 5%) of Ref. [34]. The massively multipoint optimization achieves 0.24% more fuel burn reduction, which seems to be insignificant and might be within the error bars of the BTS data. However, this is due to the choice of a concise case in this work. This case just uses simplified models, e.g., the *Luftfahrt Technischen Handbuch* (LTH) wing mass model and fixed-wing parameters (span, taper, and area). As shown in Fig. 21, different optimizations trade-off the influences of aerodynamic and structural disciplines mainly by changing the sweep angle. These simplifications limit the optimization ability in fuel burn reduction, and the exact improvement to aircraft efficiency should be evaluated in a high-fidelity multidisciplinary design optimization context [40,65]. Besides, we merely use a cruise-based estimation of the fuel burn and involve an assumption of $W_{\text{Fuel}} = 10 \times R$ to compute the cruise C_L. Yanto and Liem [44] found that the cruise-only approximation in fuel burn computation shows significant errors (greater than 30%). The optimization gains might be blurred off by the errors. Future studies should be based on more accurate fuel burn computation methods. Nevertheless, the results presented herein imply that a higher fuel efficiency of commercial aircraft can be achieved via the massively multipoint optimization.

V. Conclusions

In this paper, a surrogate-assisted gradient-based optimization architecture was proposed to strictly solve massively multipoint aerodynamic design problems with a large number of shape design variables. This architecture leverages both efficient gradient-based optimization and fast evaluations of surrogate models to reduce the computational cost.

The optimization architecture is composed of two loops. In the outer loop, a gradient-based algorithm is used to search the high-dimensional design space, which ensures efficiency. In the inner loop, GEK and POD-kriging models are constructed to predict aerodynamic functions and gradients on each design point. These surrogate models are trained in the low-dimensional space spanned by flow condition variables, where the diversity among different design points exists. This avoids the curse of dimensionality. To efficiently refine the surrogate models, an adaptive sampling criterion is proposed that is based on the estimated prediction error.

Airfoil optimization results show that the infill sampling process should not be terminated by a loose threshold, which may have the optimization terminated early. In the aerodynamic shape optimization of a commercial aircraft wing, the massively multipoint optimization reduces the fuel burn of the single-point optimal design by 0.5%, whereas only a 0.26% reduction is obtained by the multipoint optimization. This result highlights the effect and the necessity to conduct the massively multipoint optimization in aircraft design. The optimization tests also show that the proposed optimization architecture reduces the computational cost of a direct gradient-based optimization by more than one order in massively multipoint optimization problems.

The proposed optimization architecture reduces the computational cost of a massively multipoint optimization to a level close to the cost of a regular multipoint optimization. Thus, it is computationally affordable to perform aircraft design that considers hundreds or even thousands of missions simultaneously. Moreover, this architecture provides a promising approach for other high-fidelity design optimization problems that involve a large number of operating conditions and design variables. Nevertheless, its performance remains to be verified in scenarios where the number of flow condition variables is high as well. For example, aircraft design optimization with active control mechanisms places active control parameters in $\boldsymbol{x}_f$ besides the angle of attack, which leads to a higher-dimensional space. It might be challenging to solve these problems by the proposed method because more samples might be required to train an accurate surrogate model.

Appendix: Fuel Burn Estimation

Based on a Breguet range equation, the flight range R can be expressed as

$$R = \frac{V}{g}\frac{1}{\text{SFC}}\frac{C_L}{C_D}\ell_n\left(\frac{W_1}{W_2}\right) \tag{A1}$$

where V is the cruise speed, SFC is the specific fuel consumption, g is the gravitational acceleration, and C_L/C_D is the lift-to-drag ratio. W_1 and W_2 are the initial and final weights of the aircraft. W_2 is the sum of the payload (W_{Payload}), the wing (W_{Wing}), and the rest (W_{Rest}):

$$\begin{aligned} W_1 &= W_2 + W_{\text{Fuel}} \\ W_2 &= W_{\text{Payload}} + W_{\text{Wing}} + W_{\text{Rest}} \end{aligned} \tag{A2}$$

The rest weight of the aircraft is computed by using $W_{\text{Rest}} = W_{\text{OEW}} - W_{\text{Wing}}$ and Eq. (A4) with the parameters specified in Table 1. We have $W_{\text{Rest}} = (118{,}000\text{–}32{,}365)$ kg $= 85{,}635$ kg for the problem in this paper.

Then, the fuel burn of a mission with the given flight range and payload is

Table A1 Parameter description of the LTH wing mass estimation method [66,2]

Parameters	Description	Ranges
W_{wing}	Wing mass	$4100 \sim 50{,}300$ kg
A_{wing}	Wing area	$75 \sim 550$ m^2
MTOM	Maximum takeoff mass	$40{,}000 \sim 400{,}000$ kg
$(t/c)_{\text{rep}}$	Representative t/c ratio	$0.10 \sim 0.15$
AR	Aspect ratio	$6.9 \sim 9.6$
$\Lambda_{25\%}$	Quarter-chord sweep angle	$15.0 \sim 37.5$ deg

$$\begin{aligned} W_{\text{Fuel}} &= W_1 - W_2 \\ &= W_2 \exp\left(R\frac{g \times \text{SFC}}{V}\frac{C_D}{C_L}\right) - W_2 \\ &= (W_{\text{Payload}} + W_{\text{Wing}} + W_{\text{Rest}})\left(\exp\left(R\frac{g \times \text{SFC}}{V}\frac{C_D}{C_L}\right) - 1\right) \end{aligned} \tag{A3}$$

We use the LTH method [66,67], which is a statistical method for large civil transports, to estimate the wing weight:

$$\begin{aligned} W_{\text{Wing}} = {} & 2.20013 \times 10^{-4} \times (401.146 \times S_{\text{Wing}}^{1.31} + \text{MTOM}^{1.1038}) \\ & \times (t/c)_{\text{rep}}^{-0.5} \times \text{AR}^{1.5} \times \frac{1.0}{\cos \Lambda_{25\%}} \end{aligned} \tag{A4}$$

The parameters in Eq. (A4) are explained in Table A1.

The loose bounds of shape design variables would lead to unrealistic designs [26] without involving constraints on the low-speed aerodynamic performance, like $C_{L,\text{Max}}$. So, we only allow the section shape to change in a small range ($[-0.01, 0.01] \times c_{\text{local}}$), and c_{local} is the local chord length. In this circumstance, the thickness of each section does not change much, and thus $(t/c)_{\text{rep}}$ almost remains the same. We eliminate its influence on the wing weight to simplify Eq. (A4). Thus, W_{Wing} only depends on the sweep angle in this case.

Acknowledgments

This work was supported by the 111 Project of China (B17037). The authors would like to acknowledge John T. Hwang and Mohamed A. Bouhlel for the valuable suggestions in this work. The authors also acknowledge the three reviewers for their valuable and constructive comments.

References

[1] Skinner, S., and Zare-Behtash, H., "State-of-the-Art in Aerodynamic Shape Optimisation Methods," *Applied Soft Computing*, Vol. 62, Jan. 2018, pp. 933–962. https://doi.org/10.1016/j.asoc.2017.09.030

[2] Kenway, G. K. W., and Martins, J. R. R. A., "Multipoint Aerodynamic Shape Optimization Investigations of the Common Research Model Wing," *AIAA Journal*, Vol. 54, No. 1, 2016, pp. 113–128. https://doi.org/10.2514/1.J054154

[3] Li, J., Cai, J., and Qu, K., "Surrogate-Based Aerodynamic Shape Optimization with the Active Subspace Method," *Structural and Multidisciplinary Optimization*, Vol. 59, No. 2, 2019, pp. 403–419. https://doi.org/10.1007/s00158-018-2073-5

[4] Jameson, A., "Aerodynamic Design via Control Theory," *Journal of Scientific Computing*, Vol. 3, No. 3, 1988, pp. 233–260. https://doi.org/10.1007/bf01061285

[5] Nadarajah, S., and Jameson, A., "A Comparison of the Continuous and Discrete Adjoint Approach to Automatic Aerodynamic Optimization," *38th AIAA Aerospace Sciences Meeting and Exhibit*, AIAA Paper 2000-0667, 2000. https://doi.org/10.2514/6.2000-667

[6] Mader, C. A., Martins, J. R. R. A., Alonso, J. J., and van der Weide, E., "ADjoint: An Approach for the Rapid Development of Discrete Adjoint Solvers," *AIAA Journal*, Vol. 46, No. 4, 2008, pp. 863–873. https://doi.org/10.2514/1.29123

[7] Lyu, Z., Kenway, G. K., Paige, C., and Martins, J. R. R. A., "Automatic Differentiation Adjoint of the Reynolds-Averaged Navier–Stokes Equations with a Turbulence Model," *21st AIAA Computational Fluid Dynamics Conference*, AIAA Paper 2013-2581, 2013. https://doi.org/10.2514/6.2013-2581

[8] Xu, S., Jahn, W., and Müller, J.-D., "CAD-Based Shape Optimisation with CFD Using a Discrete Adjoint," *International Journal for Numerical Methods in Fluids*, Vol. 74, No. 3, 2013, pp. 153–168. https://doi.org/10.1002/fld.3844

[9] He, P., Mader, C. A., Martins, J. R., and Maki, K. J., "An Aerodynamic Design Optimization Framework Using a Discrete Adjoint Approach with OpenFOAM," *Computers and Fluids*, Vol. 168, May 2018, pp. 285–303. https://doi.org/10.1016/j.compfluid.2018.04.012

[10] Li, J., Cai, J., and Qu, K., "Adjoint-Based Two-Step Optimization Method Using Proper Orthogonal Decomposition and Domain Decomposition," *AIAA Journal*, Vol. 56, No. 3, 2018, pp. 1133–1145. https://doi.org/10.2514/1.j055773

[11] Zingg, D. W., and Elias, S., "Aerodynamic Optimization Under a Range of Operating Conditions," *AIAA Journal*, Vol. 44, No. 11, 2006, pp. 2787–2792. https://doi.org/10.2514/1.23658

[12] Lyu, Z., Kenway, G. K. W., and Martins, J. R. R. A., "Aerodynamic Shape Optimization Investigations of the Common Research Model Wing Benchmark," *AIAA Journal*, Vol. 53, No. 4, 2015, pp. 968–985. https://doi.org/10.2514/1.J053318

[13] Lyu, Z., and Martins, J. R. R. A., "Aerodynamic Design Optimization Studies of a Blended-Wing-Body Aircraft," *Journal of Aircraft*, Vol. 51, No. 5, 2014, pp. 1604–1617. https://doi.org/10.2514/1.c032491

[14] Economon, T. D., Palacios, F., Copeland, S. R., Lukaczyk, T. W., and Alonso, J. J., "SU2: An Open-Source Suite for Multiphysics Simulation and Design," *AIAA Journal*, Vol. 54, No. 3, 2016, pp. 828–846. https://doi.org/10.2514/1.j053813

[15] Kenway, G. K., Mader, C. A., He, P., and Martins, J. R., "Effective Adjoint Approaches for Computational Fluid Dynamics," *Progress in Aerospace Sciences*, Vol. 110, Oct. 2019, Paper 100542. https://doi.org/10.1016/j.paerosci.2019.05.002

[16] Martins, J. R. R. A., Sturdza, P., and Alonso, J. J., "The Complex-Step Derivative Approximation," *ACM Transactions on Mathematical Software*, Vol. 29, No. 3, 2003, pp. 245–262. https://doi.org/10.1145/838250.838251

[17] Leifsson, L., Koziel, S., and Bekasiewicz, A., "Fast Low-Fidelity Wing Aerodynamics Model for Surrogate-Based Shape Optimization," *Procedia Computer Science*, Vol. 29, 2014, pp. 811–820. https://doi.org/10.1016/j.procs.2014.05.073

[18] Koziel, S., and Leifsson, L., "Introduction to Surrogate Modeling and Surrogate-Based Optimization," *Simulation-Driven Design by Knowledge-Based Response Correction Techniques*, Springer International, New York, 2016, pp. 31–61. https://doi.org/10.1007/978-3-319-30115-0_4

[19] Han, Z., Xu, C., Zhang, L., Zhang, Y., Zhang, K., and Song, W., "Efficient Aerodynamic Shape Optimization Using Variable-Fidelity Surrogate Models and Multilevel Computational Grids," *Chinese Journal of Aeronautics* (in press). https://doi.org/10.1016/j.cja.2019.05.001

[20] Li, J., Bouhlel, M. A., and Martins, J. R. R. A., "Data-Based Approach for Fast Airfoil Analysis and Optimization," *AIAA Journal*, Vol. 57, No. 2, 2019, pp. 581–596. https://doi.org/10.2514/1.j057129

[21] Koziel, S., and Leifsson, L., "Surrogate-Based Aerodynamic Shape Optimization by Variable-Resolution Models," *AIAA Journal*, Vol. 51, No. 1, 2013, pp. 94–106. https://doi.org/10.2514/1.j051583

[22] Han, Z.-H., Abu-Zurayk, M., Görtz, S., and Ilic, C., "Surrogate-Based Aerodynamic Shape Optimization of a Wing-Body Transport Aircraft Configuration," *Notes on Numerical Fluid Mechanics and Multidisciplinary Design*, Springer International, New York, 2018, pp. 257–282. https://doi.org/10.1007/978-3-319-72020-3_16

[23] Li, J., Cai, J., and Qu, K., "Drag Reduction of Transonic Wings with Surrogate-Based Optimization," *Proceedings of the 2018 Asia-Pacific International Symposium on Aerospace Technology (APISAT 2018)*, 2018. https://doi.org/10.1007/978-981-13-3305-7_85

[24] Abbas-Bayoumi, A., and Becker, K., "An Industrial View on Numerical Simulation for Aircraft Aerodynamic Design," *Journal of Mathematics*

in Industry, Vol. 1, No. 1, 2011, Paper 10.
https://doi.org/10.1186/2190-5983-1-10

[25] Drela, M., "Pros and Cons of Airfoil Optimization," *Frontiers of Computational Fluid Dynamics 1998*, World Scientific, Singapore, 1998, pp. 363–381.
https://doi.org/10.1142/9789812815774_0019

[26] Li, J., He, S., and Martins, J. R., "Data-Driven Constraint Approach to Ensure Low-Speed Performance in Transonic Aerodynamic Shape Optimization," *Aerospace Science and Technology*, Vol. 92, Sept. 2019, pp. 536–550.
https://doi.org/10.1016/j.ast.2019.06.008

[27] Reuther, J. J., Jameson, A., Alonso, J. J., Rimlinger, M. J., and Saunders, D., "Constrained Multipoint Aerodynamic Shape Optimization Using an Adjoint Formulation and Parallel Computers, Part 1," *Journal of Aircraft*, Vol. 36, No. 1, 1999, pp. 51–60.
https://doi.org/10.2514/2.2413

[28] Li, W., Huyse, L., and Padula, S., "Robust Airfoil Optimization to Achieve Drag Reduction over a Range of Mach Numbers," *Structural and Multidisciplinary Optimization*, Vol. 24, No. 1, 2002, pp. 38–50.
https://doi.org/10.1007/s00158-002-0212-4

[29] Nemec, M., Zingg, D. W., and Pulliam, T. H., "Multipoint and Multi-Objective Aerodynamic Shape Optimization," *AIAA Journal*, Vol. 42, No. 6, 2004, pp. 1057–1065.
https://doi.org/10.2514/1.10415

[30] Toal, D. J. J., and Keane, A. J., "Efficient Multipoint Aerodynamic Design Optimization via Cokriging," *Journal of Aircraft*, Vol. 48, No. 5, 2011, pp. 1685–1695.
https://doi.org/10.2514/1.c031342

[31] Buckley, H. P., Zhou, B. Y., and Zingg, D. W., "Airfoil Optimization Using Practical Aerodynamic Design Requirements," *Journal of Aircraft*, Vol. 47, No. 5, 2010, pp. 1707–1719.
https://doi.org/10.2514/1.C000256

[32] Gallard, F., Meaux, M., Montagnac, M., and Mohammadi, B., "Aerodynamic Aircraft Design for Mission Performance by Multipoint Optimization," *21st AIAA Computational Fluid Dynamics Conference*, AIAA Paper 2013-2582, 2013.
https://doi.org/10.2514/6.2013-2582

[33] Hwang, J. T., Jasa, J. P., and Martins, J. R. R. A., "High-Fidelity Design-Allocation Optimization of a Commercial Aircraft Maximizing Airline Profit," *Journal of Aircraft*, Vol. 56, No. 3, May 2019, pp. 1164–1178.
https://doi.org/10.2514/1.c035082

[34] Liem, R. P., Kenway, G. K. W., and Martins, J. R. R. A., "Multimission Aircraft Fuel Burn Minimization via Multipoint Aerostructural Optimization," *AIAA Journal*, Vol. 53, No. 1, 2015, pp. 104–122.
https://doi.org/10.2514/1.J052940

[35] Chai, X., Yu, X., and Wang, Y., "Multipoint Optimization on Fuel Efficiency in Conceptual Design of Wide-Body Aircraft," *Chinese Journal of Aeronautics*, Vol. 31, No. 1, 2018, pp. 99–106.
https://doi.org/10.1016/j.cja.2017.10.006

[36] Liem, R. P., Mader, C. A., and Martins, J. R. R. A., "Surrogate Models and Mixtures of Experts in Aerodynamic Performance Prediction for Aircraft Mission Analysis," *Aerospace Science and Technology*, Vol. 43, June 2015, pp. 126–151.
https://doi.org/10.1016/j.ast.2015.02.019

[37] Liem, R. P., Martins, J. R., and Kenway, G. K., "Expected Drag Minimization for Aerodynamic Design Optimization Based on Aircraft Operational Data," *Aerospace Science and Technology*, Vol. 63, April 2017, pp. 344–362.
https://doi.org/10.1016/j.ast.2017.01.006

[38] Jacome, L. B., and Elham, A., "Wing Aerostructural Optimization Under Uncertain Aircraft Range and Payload Weight," *Journal of Aircraft*, Vol. 54, No. 3, 2017, pp. 1109–1120.
https://doi.org/10.2514/1.c034050

[39] Breguet, L., "Calcul du Poids de Combustible Consumme par un Avion en vol Ascendant," *Comptes Rendus de l'acadmie des sciences*, Vol. 177, 1923, pp. 870–872.

[40] Kenway, G. K. W., and Martins, J. R. R. A., "Multipoint High-Fidelity Aerostructural Optimization of a Transport Aircraft Configuration," *Journal of Aircraft*, Vol. 51, No. 1, 2014, pp. 144–160.
https://doi.org/10.2514/1.C032150

[41] Vassberg, J., Dehaan, M., Rivers, M., and Wahls, R., "Development of a Common Research Model for Applied CFD Validation Studies," *26th AIAA Applied Aerodynamics Conference*, AIAA Paper 2008-6919, 2008.
https://doi.org/10.2514/6.2008-6919

[42] Sederberg, T. W., and Parry, S. R., "Free-Form Deformation of Solid Geometric Models," *ACM SIGGRAPH Computer Graphics*, Vol. 20, No. 4, 1986, pp. 151–160.
https://doi.org/10.1145/15886.15903

[43] "US Standard Atmosphere," National Oceanic and Atmospheric Administration, 1976.

[44] Yanto, J., and Liem, R. P., "Aircraft Fuel Burn Performance Study: A Data-Enhanced Modeling Approach," *Transportation Research, Part D: Transport and Environment*, Vol. 65, Dec. 2018, pp. 574–595.
https://doi.org/10.1016/j.trd.2018.09.014

[45] He, X., Li, J., Mader, C. A., Yildirim, A., and Martins, J. R. R. A., "Robust Aerodynamic Shape Optimization—From a Circle to an Airfoil," *Aerospace Science and Technology*, Vol. 87, April 2019, pp. 48–61.
https://doi.org/10.1016/j.ast.2019.01.051

[46] Perez, R. E., Jansen, P. W., and Martins, J. R. R. A., "pyOpt: A Python-Based Object-Oriented Framework for Nonlinear Constrained Optimization," *Structures and Multidisciplinary Optimization*, Vol. 45, No. 1, 2012, pp. 101–118.
https://doi.org/10.1007/s00158-011-0666-3

[47] Kenway, G. K. W., "pyOptSparse–PYthon OPTimization (Sparse) Framework," 2018, https://github.com/mdolab/pyoptsparse [retrieved 9 Sept. 2018].

[48] Xu, J., Cai, J., Liu, Q., and Qu, K., "Flow Simulations by Enhanced Implicit-Hole-Cutting Method on Overset Grids," *Journal of Aircraft*, Vol. 51, No. 5, 2014, pp. 1401–1409.
https://doi.org/10.2514/1.c032283

[49] Zimmermann, R., "Gradient-Enhanced Surrogate Modeling Based on Proper Orthogonal Decomposition," *Journal of Computational and Applied Mathematics*, Vol. 237, No. 1, 2013, pp. 403–418.
https://doi.org/10.1016/j.cam.2012.06.010

[50] Bouhlel, M. A., and Martins, J. R. R. A., "Gradient-Enhanced Kriging for High-Dimensional Problems," *Engineering with Computers*, Vol. 35, No. 1, 2018, pp. 157–173.
https://doi.org/10.1007/s00366-018-0590-x

[51] Lee, A., "pyswarm: Particle Swarm Optimization (PSO) with Constraint Support [online database]," 2018, https://pythonhosted.org/pyswarm [retrieved 19 Aug. 2018].

[52] Hwang, J. T., and Martins, J. R., "A Fast-Prediction Surrogate Model for Large Datasets," *Aerospace Science and Technology*, Vol. 75, April 2018, pp. 74–87.
https://doi.org/10.1016/j.ast.2017.12.030

[53] Krige, D. G., "A Statistical Approach to Some Basic Mine Valuation Problems on the Witwatersrand," *Journal of the Chemical, Metallurgical and Mining Society*, Vol. 52, No. 6, 1951, pp. 119–139.

[54] Bouhlel, M. A., Bartoli, N., Otsmane, A., and Morlier, J., "Improving Kriging Surrogates of High-Dimensional Design Models by Partial Least Squares Dimension Reduction," *Structural and Multidisciplinary Optimization*, Vol. 53, No. 5, 2016, pp. 935–952.
https://doi.org/10.1007/s00158-015-1395-9

[55] Liu, J., Song, W.-P., Han, Z.-H., and Zhang, Y., "Efficient Aerodynamic Shape Optimization of Transonic Wings Using a Parallel Infilling Strategy and Surrogate Models," *Structural and Multidisciplinary Optimization*, Vol. 55, No. 3, 2016, pp. 925–943.
https://doi.org/10.1007/s00158-016-1546-7

[56] Jones, D. R., Schonlau, M., and Welch, W. J., "Efficient Global Optimization of Expensive Black-Box Functions," *Journal of Global Optimization*, Vol. 13, No. 4, 1998, pp. 455–492.
https://doi.org/10.1023/A:1008306431147

[57] Mardia, K. V., and Watkins, A. J., "On Multimodality of the Likelihood in the Spatial Linear Model," *Biometrika*, Vol. 76, No. 2, 1989, pp. 289–295.
https://doi.org/10.1093/biomet/76.2.289

[58] Xiao, M., Breitkopf, P., Coelho, R. F., Knopf-Lenoir, C., Sidorkiewicz, M., and Villon, P., "Model Reduction by CPOD and Kriging," *Structural and Multidisciplinary Optimization*, Vol. 41, No. 4, 2009, pp. 555–574.
https://doi.org/10.1007/s00158-009-0434-9

[59] Lappo, V., and Habashi, W., "Reduced Order Pod/Kriging Modeling for Real-Time 3D CFD," *11th Pan-American Congress of Applied Mechanics*, 2010.

[60] Braconnier, T., Ferrier, M., Jouhaud, J.-C., Montagnac, M., and Sagaut, P., "Towards an Adaptive POD/SVD Surrogate Model for Aeronautic Design," *Computers and Fluids*, Vol. 40, No. 1, 2011, pp. 195–209.
https://doi.org/10.1016/j.compfluid.2010.09.002

[61] Chiplunkar, A., Bosco, E., and Morlier, J., "Gaussian Process for Aerodynamic Pressures Prediction in Fast Fluid Structure Interaction Simulations," *Advances in Structural and Multidisciplinary Optimization*, Springer International, New York, 2017, pp. 221–233.
https://doi.org/10.1007/978-3-319-67988-4_15

[62] Sasena, M. J., Papalambros, P., and Goovaerts, P., "Exploration of Metamodeling Sampling Criteria for Constrained Global Optimization," *Engineering Optimization*, Vol. 34, No. 3, 2002, pp. 263–278.
https://doi.org/10.1080/03052150211751

[63] Clark, D. L., Bae, H., Deaton, J. D., and Forster, E. E., "Adaptive Infill Criteria for Non-Deterministic Kriging Considering Aleatory and Epistemic Uncertainties," *AIAA Scitech 2019 Forum*, AIAA Paper 2019-1489, 2019.
https://doi.org/10.2514/6.2019-1489

[64] Bartoli, N., Lefebvre, T., Dubreuil, S., Olivanti, R., Priem, R., Bons, N., Martins, J., and Morlier, J., "Adaptive Modeling Strategy for Constrained Global Optimization with Application to Aerodynamic Wing Design," *Aerospace Science and Technology*, Vol. 90, July 2019, pp. 85–102.
https://doi.org/10.1016/j.ast.2019.03.041

[65] Martins, J. R. R. A., and Lambe, A. B., "Multidisciplinary Design Optimization: A Survey of Architectures," *AIAA Journal*, Vol. 51, No. 9, 2013, pp. 2049–2075.
https://doi.org/10.2514/1.J051895

[66] Dorbath, F., "Civil Jet Transport Aircraft-Statistical Mass Estimation," Luftfahrttechnisches Handbuch: MA, Vol. 401, 2011, pp. 12–01.

[67] Mariens, J., Elham, A., and van Tooren, M. J. L., "Influence of Weight Modelling on the Outcome of Wing Design Using Multidisciplinary Design Optimisation Techniques," *Aeronautical Journal*, Vol. 117, No. 1195, 2013, pp. 871–895.
https://doi.org/10.1017/s0001924000008563

K. E. Willcox
Associate Editor